IEEE Access
Multidisciplinary | Rapid Review | Open Access Journal

Received May 2, 2020, accepted May 27, 2020, date of publication June 1, 2020, date of current version July 1, 2020.

Digital Object Identifier 10.1109/ACCESS.2020.2999202

Autonomous Self-Reconfigurable Floor Cleaning Robot

RIZUWANA PARWEEN[1], (Member, IEEE), MANUEL VEGA HEREDIA[2], MADAN MOHAN RAYGURU[1], RAIHAN ENJIKALAYIL ABDULKADER[1], AND MOHAN RAJESH ELARA[1]

[1]Engineering Product Development, Singapore University of Technology and Design, Singapore 487372
[2]Apt of Engineering and Technology, Universidad Autonoma de Occidente, Los Mochis 81223, Mexico

Corresponding author: Rizuwana Parween (rizuwana_parween@sutd.edu.sg)

This work was supported in part by the National Robotics Program through the Robotics Enabling Capabilities and Technologies (Funding Agency) under Project 192 25 00051, in part by the National Robotics Program through the Robot Domain Specific (Funding Agency) under Project 192 22 00058, and in part by the Agency for Science, Technology and Research.

ABSTRACT The cleaning robots are going through some significant development in recent years, driven by the greater market penetration and the demand for better cleaning performance. However, most of the robots have problems covering the total cleaning area given geometric limitations of the platforms in relation to the cleaning stage, given furniture and architecture. In this paper, we describe the hTrihex platform, which is a self-reconfigurable adaptive robot that attains three different configurations. The change in configuration gives rise to variation in the kinematic model, which in turn changes the behavior of robot locomotion. The change in configuration and the robot position is evaluated using the measurements from the on-board sensors like the encoders, LIDAR, and inertial measuring unit (IMU). These data are then utilized to develop a new cascade control strategy for motion control of h-Trihex. The control cascade comprises of a robust backstepping controller in the outer loop for tackling the varying kinematic and a conventional PID in the inner loop for speed control. This cascade is appended by a PID controller, for correcting the wheel orientation after each configuration change. The proposed design assures asymptotic path tracking and satisfactory closed-loop performance, which are validated through numerical simulations and experiments.

INDEX TERMS Self-reconfigurable robot, polyhex, differential based kinematics model, independent steering wheel drive, tiling robot, Lyapunov stability theory.

I. INTRODUCTION

Cleaning has been an essential and important part of our lives, which has evolved and improved over time. Today's busy lifestyle has led to an increased demand for automated floor cleaning robots with fully automatic functions. In developing countries, autonomous floor cleaning robots are majorly used in smart homes, residential and office spaces to clean the floor. As per the global market study, there is a huge demand for the application these robots in domestics setting with fully automated features and the least human assistance and these robots still constitute a minute market share of the global vacuum cleaner market, but their recognition and adoption is growing at a significant pace. iRobot Corporation, Neato Robotics, Dyson Ltd., Samsung Electronics Company Ltd., LG Electronics Inc, and Panasonic Corporation are the key players in the global autonomous floor-cleaning robot market. These robots are compact and perform the assigned cleaning task without human intervention [1]. For area coverage during cleaning, these robots follow the motion planning algorithms, including backtracking spiral motion, spiral motion, and boustrophedon motion (back and forth) and simple zig-zag motion patterns. These existing robots are of standard configuration (either circular or D shaped), and they fail to reach the corners, concave spaces, convex regions in the cleaning environment. For effective cleaning, the user has to manually rearrange the furniture setting to clear the navigation path of the robot. Even though a proper path planning and motion capabilities are added to a fixed configuration robots, these robots may need more time and energy to perform the complex task efficiently, compared to the reconfigurable counterparts. Therefore, the cleaning

The associate editor coordinating the review of this manuscript and approving it for publication was Huiyu Zhou.

performance of the robots can be enhanced by developing a reconfigurable robot that adapt various configurations to reach inaccessible spaces in the cleaning workspace.

The concept of reconfigurable robots have been used in space exploration and remote environment and these robots are usually composed of several modules and have the ability to adapt in a new environment by changing the shape and recover from damage. Literature reveals that polybot, MTran III, Molecubes, Omni-Pi-tent, Sambot, and Symbrion are the promising selfreconfigurable robots with variable morphology [2]–[6]. Our research team is the pioneer in applying the concept of the self-reconfiguratibility for the floor cleaning application. We have developed various polyform based self-reconfigurable robotic platforms, including the hTetro, hTetrkis, hHoneycomb, and hTetran [7]–[10]. All these platforms are able to attain multiple configurations as per the planar hinge dissection principle. These robots follow tiling based path planning techniques for area coverage. Our study shows that the platform achieves better area coverage performance with tilling based path planning than the fixed morphology cleaning robot.

The hTetro platform is the first of kind self-reconfigurable robot that consists of four rectangular blocks connected through revolute joints and attains seven distinct configurations. All these configurations are of regular geometric patterns which help to access the spaces with 90 degrees included angles. In different iterations of hTetro, our team have extensively studied the platform's performance by incorporating different locomotion principle (differential drive, single wheel contact), hinge mechanism (servo based, electromagnetic and passive), controller design and tiling path planning algorithm. Tun *et al.*, proposed a simplified open-loop kinematics controller for hTetro with four-wheel independent steering wheel drive mechanism [11]. Yuyao *et al.*, suggested instantaneous curvature rotation based closed-loop kinematics for hTetro platform having each block with steerable differential drive in each block [12]. Le *et al.*, also proposed the A-star based zigzag path planning algorithm and Genetic Algorithm of the Traveling Salesman Problem for this class of robots and tested the area coverage performance [13]–[17]. The experimental results showed the superior area coverage performance of the platform in real-time scenarios of the cleaning environmental.

To access the convex (included angle more than 90 degree) and concave corners (included angle less than 90 degree), we have developed another platform called 'hTetrakis', that consists of four moniamonds (equilateral triangles) joined by revolute joints. By altering the position and alignment of these moniamonds, the platform attains three distinct configurations [18]–[20]. The motion controller of the platform is based on the three omnidirectional wheels arranged in a triangular fashion [8]. For accessing circular spaces, arcs, and covering unstructured environment, we have developed another polyform based platform called the 'hHoneycomb' which consists of four regular hexagonal blocks [9]. This platform adapts seven distinct shapes which has arc and convex shapes. The locomotion of the platform is achieved by incorporating four omnidirectional wheels in the middle blocks. Each middle block consists of two omnidirectional wheels arranged in horizontal and vertical direction. During navigation of the platform between two waypoints, the robot undergoes horizontal movement followed by vertical movement or vice versa. With few configurations, we observed that the platform undergoes huge heading error during the locomotion along the horizontal and vertical direction. This error is mainly due to the 120 degree included angle between the wheels.

For these polyform based tiling robots, point to point navigation along a straight line can be achieved by using either a differential drive or four-wheel independent steering drive in each block. As the control parameters in differential based wheel layout in each block has more number of control parameters which demands complex controller design, the independent steering based wheel layout is preferred. Secondly, in a dynamic environment, there is a need of robust controller and flexible design of the platform that can access convex, concave, arch, and circular spaces. Considering all these factors, we have developed a compact polyhex based platform called 'hTrihex,' consisting of three hexagonal blocks connected with two revolute hinged. The platform can change any of its three configurations with an objective of following both convex and concave spaces in the environment. Out of three hexagonal blocks, two blocks have independent steering wheels, and the locomotion of the entire platform follows a differential drive principle. For different configurations, the platform undergoes a differential drive-based locomotion with a variable wheel to wheel distance.

In general robots, dynamics are modeled as multiple-input multiple-output (MIMO) systems [21]. As the robot changes configurations according to environmental changes, the shape and kinematics of the robot also change. Therefore, the kinematics based robot motion control has to be robust against the changes in mathematical model [22]. For the purpose, the kinematics is expressed in the polar form, and a robust backstepping technique is proposed to derive the control inputs. This outer kinematic control loop is followed by a conventional speed control loop using the PID technique. The effectiveness of the overall control cascade is validated by numerical simulations and experiments. This paper outlines the robot architecture, kinematic modeling, controller design with simulated results. In addition, it describes real-time experimental results for synchronization of heading angle with steering angle, heading angle controller, path following with autonomy.

This paper describes the detailed design, development and control architecture of a hTrihex tiling robot. Section II, III, IV outline the platform architecture, kinematic modelling, and controller design of the platform, respectively. Section V and VI describes the results and conclusion, respectively.

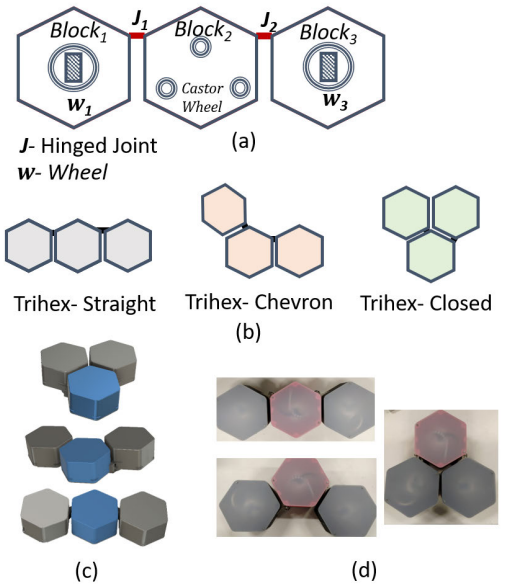

FIGURE 1. (a) Schematic layout (b) CAD model, and (c) prototype of the hTrihex platform.

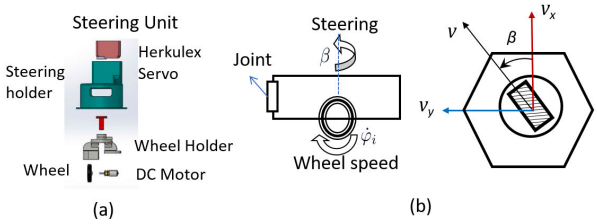

FIGURE 2. (a) CAD module of the Steering module (b) kinematics diagram of the steering module of the hTrihex platform.

II. PLATFORM ARCHITECTURE

The hTrihex platform consists of three hexagonal blocks connected by active revolute hinges. The $block_1$ and $block_2$ are connected at joint J_1 and the $block_2$ and $block_3$ are connected at joint J_2, as shown in Fig 1. The base of the platform is made of an acrylic plate that is easily detachable. The sidewalls, the steering unit, and the motor holder are fabricated using PLA material in 3D Printer. The side walls modular and are attached with the slot and hence completely eliminate the need of fasteners. Each hinge comprises a herkulex servo motor that provides planar rotation of the block and revolute hinge, and as a result, the platform can achieve three configurations including the straight, chevron, and closed shape, as shown in Fig. 1. These configurations help the platform to access both narrow spaces with an included angle of more than 90 degrees and curved spaces in the environment.

The platform locomotion is based on differential drive principle with two independent wheel modules in $block_1$ and $block_3$. Each wheel module has a separate herkulex servo motor for steering motion and a DC motor attached to the wheel for the rotational movement of the wheel, shown in Fig. 2. The locomotion of the robot is achieved by the steering mechanism where the herkulex servo changes

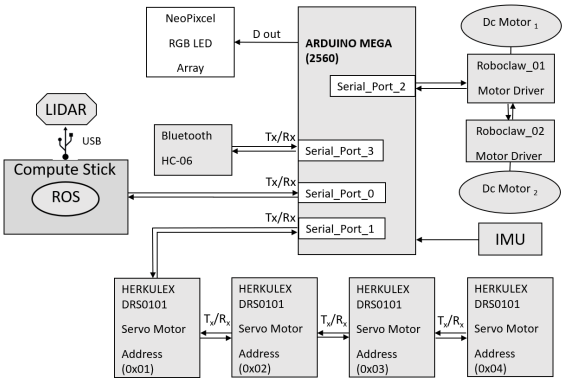

FIGURE 3. Block diagram of the electronics module of the hTrihex platform.

the orientation of the wheel. Each wheel (32 mm diameter, 90-degree output, with the gear ratio of 200:1) is connected to a dc motor having the maximum speed of 250 rpm at 5v. Roboclaw is used in the each side block to provide the 5v supply to the DC motor. In the middle, block is mounted the caster wheels that provide stability to side blocks during reconfiguration. An Arduino Mega micro-controller is used to control the entire operation. The microcontroller is placed in $block_2$, and the power source of 7.4v battery is placed in block $block_3$.

The block diagram of the electronic layout of the platform is shown in Fig. 3. A Lidar is mounted on $block_2$ to achieve autonomous navigation. The use of LIDAR may be expensive, but it can be advantageous in 3-dimensional perception (which is shown in few previous works). Intel compute stick is used as a microprocessor to map the environment based on the Lidar output. Arduino is connected to compute stick using usb serial, compute stick uses ROS platform to establish a proper communication interface with Lidar and Arduino. In this system, Arduino works in slave mode and Compute stick as the master. Based on the Lidar values compute stick sends navigation commands to the Arduino to achieve area coverage for the given space. Lidar sends the data via TX communication Port and Receive data via RX port as shown in Fig. 3.

The control architecture of this platform comprises an upper layer of autonomy for path planning and a lower layer of locomotion control. The autonomy layer, running on Intel Compute Stick, creates the map of the environment using Lidar and sets the tiling patterns using tiling based path planning theorems, described in the next section. From the generated map, the total no of grids that occupies is extracted. As the hTrihex platform has three hexagonal blocks, it can cover three distinct grids at any point of time. During reconfiguration, the middle block remains fixed, and hence the grid containing the middle block is always considered as the reference point (waypoint). Each waypoint stores the information about the platform coordinates and the corresponding configuration. In the constructed map, the path is generated together with required configurations based on the

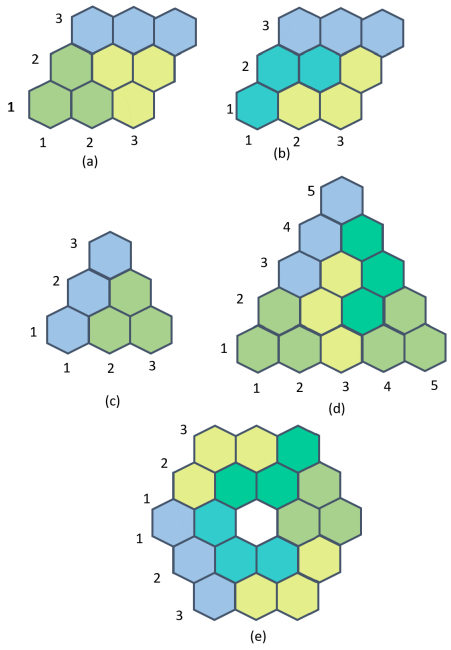

FIGURE 4. Different regular hexagon based workspace in the form of (a) 'Hexagonal Rectangle', (b) 'Hexagonal Triangle',(c) 'Honeycomb'.

minimization of navigation energy. The navigation energy includes the energy consumption during reconfiguration, in-plane pivot, and translation between the waypoints.

The autonomy layer, upon executing the main algorithm, extracts data of x, y coordinates, the sequence of waypoints, and steering angle required for the platform, and the motion planner helps the platform to traverse between the two consecutive waypoints. It prioritizes the shapeshifting and change of steering angle before it proceeds on to the moving process. Through Arduino Mega located in the middle module, the locomotion layer, using the kinematic model, calculates the required velocities of the differential drive of the platform. Each steering angle extracted from the autonomy layer is fed back to Arduino, which then maintains the synchronized steering angle for blocks. The wheel velocities are executed and regulated individually in a RoboClaw motor controller in each module. A robust backstepping controller (Section V) with feedback from an inertial measuring unit is used to achieve the stable locomotion while moving from one waypoint to another waypoint, maintaning a desired heading.

III. COVERAGE PATH PLANNING BASED ON hTrihex

The hTrihex platform tiles the predescribed environment with three configurations and the trihex based tiling theorems are described as follows.

Theorem 1: A hexagonal rectangle of side 3, consists of nine hexagons and it can be filled with only forms of hTrihex, shown in Fig. 4 (a) and 4 (b). A hexagonal rectangle of side n, consists of n^2 hexagons. It can be tiled with all the configurations of hTrihexes if (and only if) the total number of triangles n^2 is a multiple of three and $n > 3$. For example, a hexagonal rectangle of side 6, consists of thirty-six hexagons, and it can be filled with all forms of hTrihex.

Theorem 2: A hexagonal triangle of side $n = 2$ can be tiled with only two configurations of trihexes, shown in Fig. 4 (c). A hexagonal triangle of side n, consists of $n(n+1)/2$ number of triangles. It can be tiled with all the configurations of trihexes if (and only if) the total number of hexagons $n(n+1)/2$ is a multiple of 3 and $n > 3$, shown in Fig. 4 (d).

Theorem 3: A honeycomb with side 3, consists of nineteen hexagons. It can be tiled with all the configurations of trihexes with a hole at middle, as shown in Fig. 4 (e).

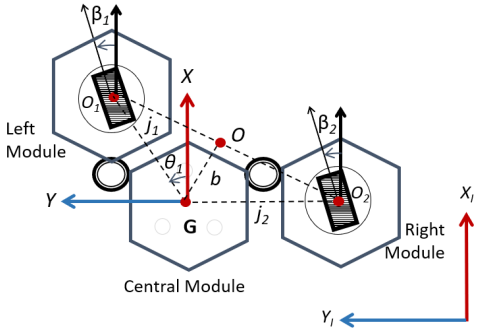

FIGURE 5. Schematic of the hTrihex platform showing the wheel layout and coordinate reference frames.

IV. KINEMATIC MODELLING

The hTrihex platform has translational, pivot-turning, and shapeshifting mode of locomotion. For a better understanding of the kinematics of the robot platform, the motion has decoupled into two modes, i.e., locomotion and reconfiguration mode. It is due to the fact that both modes of operation happen at different time instances during navigation. The platform undergoes shapeshifting followed by the locomotion of the platform. The following assumptions are made while formulating the robot's kinematic model. (1) The wheel maintains single point contact with the motion plane, and the locomotion is restricted to the planar surface. (2) The wheels are rigid, and the surface is flat and non-deformable. (3) The axis of the wheel rotation is parallel to the plane of the motion. (4) The motion of the wheel is assumed to be pure rolling without any slip.

An inertial reference frame, XYZ_I, is attached to the $X_I Y_I$ plane of motion of the robot, shown in Fig. 5. During locomotion, the platform has three degrees of freedom, i.e., the translational motion along X_I and Y_I axes, and orientation about Z_I-axis. The platform consists of three distinct k^{th} forms (k = straight,closed, and chevron). Each block is a hexagonal block with each side 'a'. A robot reference frame XYZ is attached at the center of gravity (CG), c, with Z axis parallel to Z_I axis of the fixed frame of reference, as per the right-hand coordinate system. For different configuration, the platform undergoes differential drive-based locomotion with a variable wheel to wheel distance, shown in Fig. 6. x_i, y_i is the position of the point of contact of i_{th}

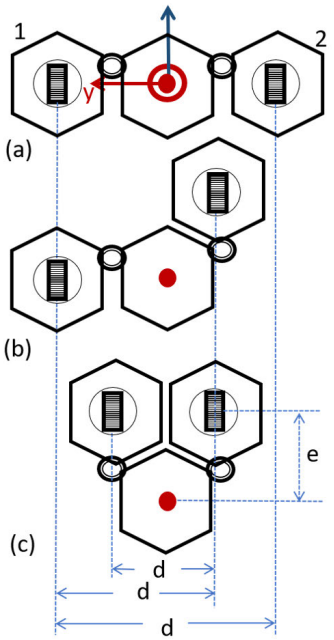

FIGURE 6. Schematic diagram of the (a) straight, (b) chevron, (c) closed configurations of the platform showing the variation of wheel distance.

($i = 1 =$ left module, and $i = 2 =$ right module) wheel module with respect to the central module. θ_1 and θ_2 are the angle of the center of the left and right wheel module with respect to the center of the central module, respectively, as shown in Fig. 5. Figure 6 shows the wheel to wheel distance for three configurations of the platform. The position of i_{th} wheel module and the variation of the wheel to wheel distance of the platform, are given by Equation (1). $j_1 =$ Distance of the left wheel module from the central module.

$j_2 =$ Distance of the right wheel module from the central module.

$2l_k =$ The distance between wheels in k_{th} configuration.

$d =$ The horizontal component of the wheel to wheel distance.

$e =$ The vertical component of the wheel to wheel distance.

$$\begin{aligned} x_i &= j_i \cos\theta_i \\ y_i &= j_i \sin\theta_i \\ d &= j_1 \sin\theta_1 + j_2 \sin\theta_2 \\ e &= j_1 \cos\theta_1 + j_2 \cos\theta_2 \\ 2l_k &= {j_1}^2 + {j_2}^2 + 2j_1 j_2 \sin(\theta_1 + \theta_2) \end{aligned} \tag{1}$$

The point 'o', is the midpoint of the distance between the two wheels. This midpoint is a virtual point whose position keeps on changing during reconfiguration. Let $\dot{\phi}_l$ and $\dot{\phi}_r$ are the angular velocity of the left and right wheel, respectively. v_l, v_r, v_c and v_o linear velocity of the left wheel, right wheel, platform and the wheel midpoint, respectively. β_1 and β_2 are the steering angle of the left and right wheel module, respectively. r is the radius of the wheel. ϕ is the orientation of the platform about the midpoint 'c' with respect to Z_I axis.

The mid point o is at a distance of b from the CG location 'c' of the platform. x_c, y_c are the position of the CG location of the k_{th} configuration. x_o, y_o are the position of the midpoint of the wheel to distance of the k_{th} configuration. The platform velocity in inertial reference frame is given Equation (2). The velocity of the wheels with respect to the CG location of the platform is given by Equation (3. Equation (4) and (5) present the constraint equations and kinematic equations respectively.

$$\begin{aligned} \dot{x}_c &= \dot{x}_o + b\dot{\phi}\cos\phi \\ \dot{y}_c &= \dot{x}_o - b\dot{\phi}\sin\phi \end{aligned} \tag{2}$$

$$r\dot{\theta}_l = \dot{x}_c\cos\phi + \dot{y}_c\sin\phi - l_k\dot{\phi} \tag{3}$$

$$r\dot{\theta}_r = \dot{x}_c\cos\phi + \dot{y}_c\sin\phi + l_k\dot{\phi} \tag{4}$$

$$-\dot{x}_c\sin\phi + \dot{y}_c\cos\phi + b\dot{\phi} = 0 \tag{5}$$

$$\begin{bmatrix} \dot{x}_c \\ \dot{y}_c \\ \dot{\phi} \end{bmatrix} = \begin{bmatrix} \frac{r}{2}\cos\phi & \frac{r}{2}\sin\phi \\ \frac{r}{2}\sin\phi & \frac{r}{2}\cos\phi \\ \frac{r}{2l_k} & \frac{r}{2l_k} \end{bmatrix} \begin{bmatrix} \dot{\phi}_l \\ \dot{\phi}_r \end{bmatrix}$$

V. CONTROLLER DESIGN

As discussed earlier section, the platform's mobility can be controlled based on differential principle. By changing the wheel's steering angle, all the three configurations of the platforms have the instantaneous center of rotation (ICR) either on the platform's body or outside the platform. Figure 7 shows the position of the ICR of three configurations. In case of the closed configuration, both wheels have to be steered by thirty degree, so that the closed configuration have ICR which is constrained to lie along a line. Without any modification of the wheel steering angles, the ICR lies at a specific point on the platform and hence the platform can undergo pivot rotation.

Each configuration of the platform traverses in a straight trajectory only if both wheels maintain the same steering angle and rotate in the same direction at equal speed. An error in wheel speeds, the steering angle adjustment, uneven load distribution causes the robot to move with a curved trajectory and deviate from the straight path. The challenge here is to reach the desired waypoint without any distance error and heading error. In addition, the controller has to maintain the steering angle the same as the heading angle. During this navigation process, the desired heading angle is estimated from the consecutive waypoints. This information is fed into the controller of each module. The changing shape of the re-configurable robots poses a unique challenge to design the controller. As the shape shifts from one configuration to another, so does the kinematics associated with it.

Figure 8 describes the control framework for hTrihex platform, which consists of a low-level controller for desired wheel velocity and a kinematic based controller for regulating the heading angle. The low-level controller is a PID controller with feedback about the angular velocity of the wheel. The encoders mounted on the wheel axles measure the angular velocity of each wheel. This control law estimates the error

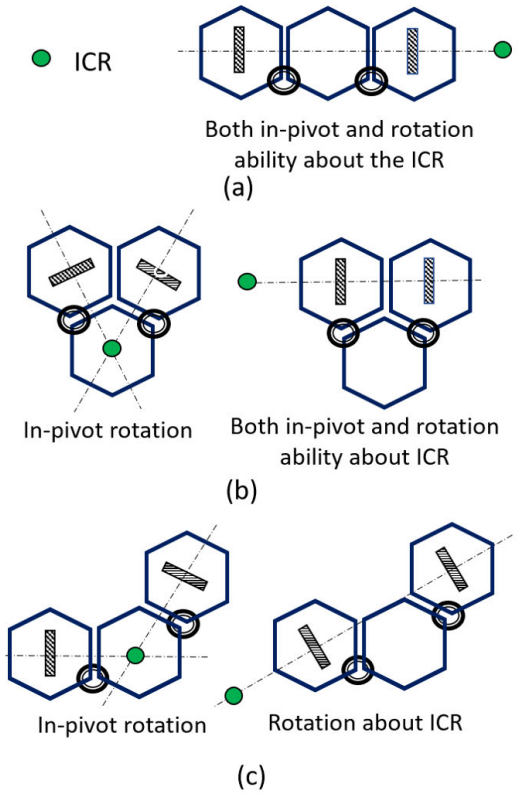

FIGURE 7. In-pivot rotation and rotation about ICR for (a) straight (b) closed and (c) chevron configuration.

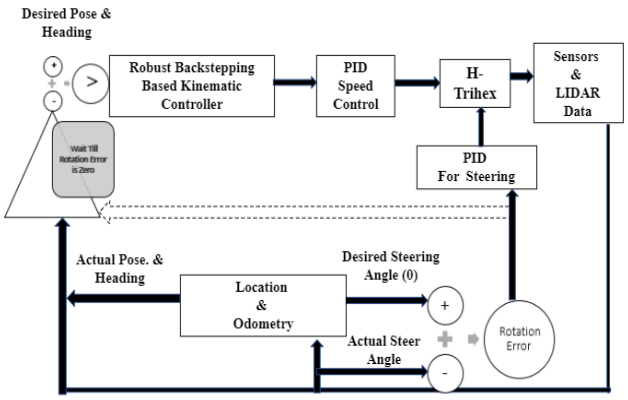

FIGURE 8. Control architecture of the hTrihex platform.

between the desired and actual wheel velocity, and then computes the required control signal to move the wheel at the desired velocity. The heading controller consists of an IMU sensor that maintains the desired heading angle. It regulates the desired angular velocity of each configuration to generate the corresponding angular velocity each wheel. The platform used LIDAR for state estimation.

Apart from the path tracking cascade (backstepping + PID for speed), the proposed design also takes care of configuration changes (Fig. 5). It should be noted that any configuration change automatically changes the wheel alignment. Which, in turn, may result in a faulty path following. Therefore, the wheels should be aligned properly every-time a configuration change occurs. The misalignment between wheels is captured by the encoders associated with the steering motor. The steering encoder data are exploited to evaluate the misalignment/rotation error. A PID controller is utilized to act upon the rotation error. Moreover, the path tracking cascade will not be able to achieve it's objective unless the wheels are aligned. So, the path tracking controller is super-ceded by the steering controller, and will not act upon till the rotation error is zero.

For this robot, the proposed motion controller is designed using the polar coordinates. This controller's outputs are the desired linear and angular velocities. The desired velocities act as the references for the inner PID loop. As the inner PID loop for speed controller is extensively discussed in robotics literature, we shall only concentrate our discussions on the outer kinematics based control loop. The kinematics of the robot follows the same differential equations, which are used for the conventional differential drive robots. However, the exact model changes due to change in shape. The kinematics of a conventional differential drive robot in polar coordinates can be written as:

$$\begin{aligned} \dot{\rho} &= -v\cos(\phi) \\ \dot{\phi}_e &= -\omega + \frac{v\sin(\phi_e)}{\rho} \end{aligned} \tag{6}$$

where ρ is the difference between the current position and the desired position, whereas ϕ_e represents the error in heading of the robot to the desired orientation. The control inputs for this model are the desired linear velocity $v = r\frac{\dot{\phi}_l+\dot{\phi}_r}{2}$, and the desired angular velocity $\omega = r\frac{\dot{\phi}_l-\dot{\phi}_r}{d}$. As the robot changes shape, the parameter d changes, and the kinematics also changes with it (even though the structure remains similar to Equation (6)). The change in shape also changes the distance between two wheels, and hence directly affects the variable $\omega(t)$. This, in turn, has the potential to affect the heading angle and linear velocity. The kinematic model with the uncertainties can be expressed as:

$$\begin{aligned} \dot{\rho} &= -v\cos(\phi_e) + D_1(\rho, v, \omega) \\ \dot{\phi}_e &= -\omega + \frac{v\sin(\phi_e)}{\rho} + D_2(\rho, v, \omega) \end{aligned} \tag{7}$$

where the variables $D_1(.)$, $D_2(.)$ may represent the unknown lumped uncertainties. A robust backstepping methodology is proposed to stabilize, given by Equation (7), for which one assumption is needed.

Assumption 1: There exist two positive scalars d_1, d_2 such that, the uncertainties are upper bounded by:

$$||D_1(.)|| \leq d_1, \quad ||D_2(.)|| \leq d_2.$$

A. CONTROL SCHEME

Let's choose a candidate Lyapunov function

$$V_1 = \frac{1}{2}\rho^2.$$

The time derivative of V_1 along the ρ dynamics can be derived as

$$\begin{aligned}\dot{V}_1 &= \rho(-v cos(\phi_e) + D_1(\rho, v, \omega)) \\ \text{Choose, } v &= k_1 \rho cos(\phi_e) + k_2 \rho + \frac{k_3}{cos(\phi_e)} tanh(\rho) \\ \dot{V}_1 &\leq -k_2 \rho^2 - k_1 \rho^2 \, cos^2(\phi_e) \\ &\quad - k_3 \rho tanh(\rho) + ||\rho D_1(.)||\end{aligned}$$

where k_1, k_2, k_3 are positive scalars. If $k_3 \geq d_1$, then

$$\dot{V}_1 \leq -k_2 \rho^2 - k_1 \rho^2 \, cos^2(\phi_e) - k_3 ||\rho|| + ||\rho|| d_1$$

which becomes negative semi definite.

Similarly, a candidate Lyapunov function $V_2 = \frac{1}{2}\phi_e^2$ can be chosen, and it can be prove that for $\omega = k_4 \phi_e + k_1 \, sin(\phi_e) cos(\phi_e) + k_2 \, sin(\phi_e) + \frac{k_3}{\rho} tan(\phi_e) tanh(\rho) + k_5 \, tanh(\phi_e)$, the time derivative of V_2 is negative semi definite, if $k_4 > 0$ and $k_5 > d_2$, i.e.,

$$\dot{V}_2 = \phi_e(-\omega + \frac{v sin(\phi_e)}{\rho} + D_2(\rho, v, \omega)) \Rightarrow \dot{V}_2 \leq 0.$$

Theorem 3: Let assumption 1 holds true for the kinematic model (7). Provided the control input v, ω are chosen as:

$$v = k_1 \rho cos(\phi_e) + k_2 \rho + \frac{k_3}{cos(\phi_e)} tanh(\rho) \tag{8}$$

$$\begin{aligned}\omega &= k_4 \phi_e + k_1 sin(\phi_e) cos(\phi_e) + k_2 sin(\phi_e) \\ &\quad + \frac{k_3}{\rho} tan(\phi_e) tanh(\rho) + k_5 \, tanh(\phi_e)\end{aligned} \tag{9}$$

then robot position and head-angle asymptotically converge to the desired position and orientation.

Proof: Choose a combined Lyapunov function $W = V_1 + V_2$. The rate of change of W along the trajectories can be given by $\dot{W} = \dot{V}_1 + \dot{V}_2$. Proceeding in a similar manner as given in the above subsection, and choosing the control inputs according to Equations (8) and (9), one can arrive at the required result.

Analytic Comparison: As the reconfigurable robots differ in shape, size and configuration depending on their purposes, many controllers have been proposed for them. A two layer PID is generally used for assuring proper set point tracking, but the performance may degrade in presence of non-linearity in the robots. A sliding mode control technique can deal with the uncertainties, but require a regular form of the system dynamics. Therefore, a backstepping based design is proposed, which can simultaneously handle the dynamical structure, and system uncertainties.

VI. RESULTS AND DISCUSSION

A. SIMULATION

The performance of the proposed controller is verified by carrying out simulation for trajectory and closed loop error while tracking a square wave. To verify the effectiveness of the control laws, the desired path is selected to be a square one. The square path can be generated by choosing the desired coordinated as (0, 2, pi/2): (2, 2, pi): (0, 2, −pi/2): (0.1, 0, 0). The initial conditions are taken as (0, 0, 0), and the desired coordinates are run for 10 secs each. The closed-loop trajectories can be followed from the Fig. 9 and Fig. 10.

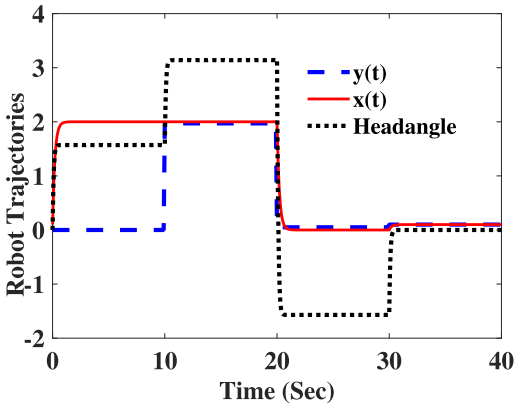

FIGURE 9. Closed loop trajectories for a square path tracking.

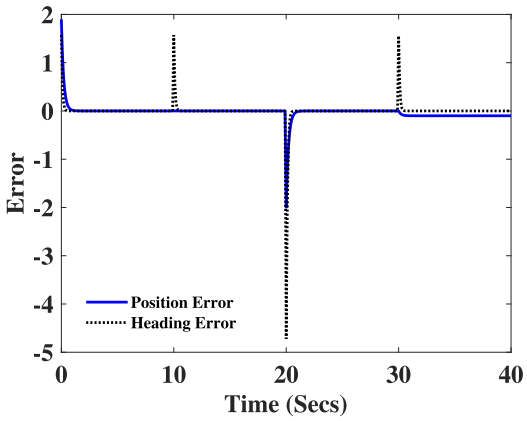

FIGURE 10. Closed loop error in position and heading angle.

It can be observed from Fig. 9 that, the robot trajectories (in Cartesian coordinates) converge to the desired values required for square path tracking. The error convergence in polar coordinates for path tracking is shown in Fig. 10. Sometimes, the head-angle needs to change continuously for circular or elliptical path tracking. To show the efficiency of the controller for such situations, the desired head angle is chosen to be a ramp signal, and then suddenly change to a fixed step signal. The closed-loop simulation can be observed in Fig. 11. Figure 12 shows the closed-loop tracking for a circular path with a configuration change. For this purpose, a constant head-angle reference is given, and the desired positions (x-y coordinates) are given in the form of periodic signals. The configuration changes two times during the path tracking, and the effect can be observed from the figure by looking at the small deviations from the reference path. However, the robot realigns to the desired path after a small amount of time. It can be concluded that the controller is robust against such configuration changes and able to satisfactorily complete the tracking goal.

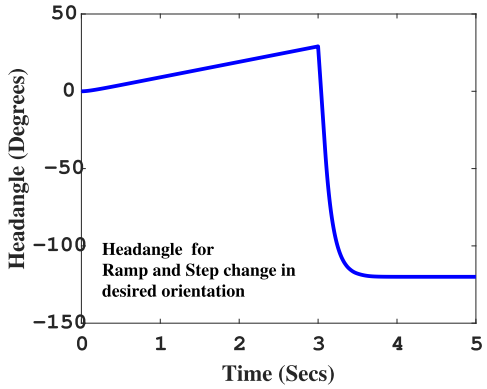

FIGURE 11. Head-angle tracking for ramp and step change in desired orientation.

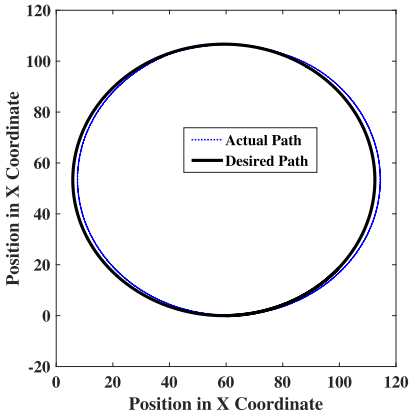

FIGURE 12. Circular path tracking.

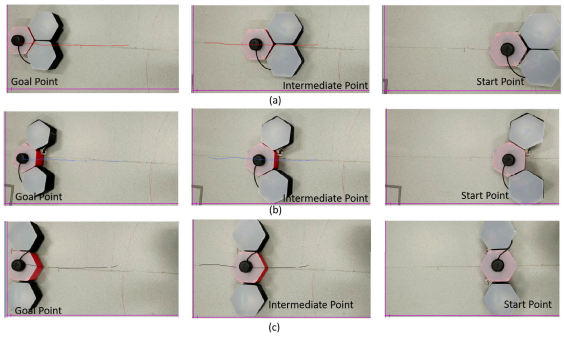

FIGURE 13. Platform position at different time instant.

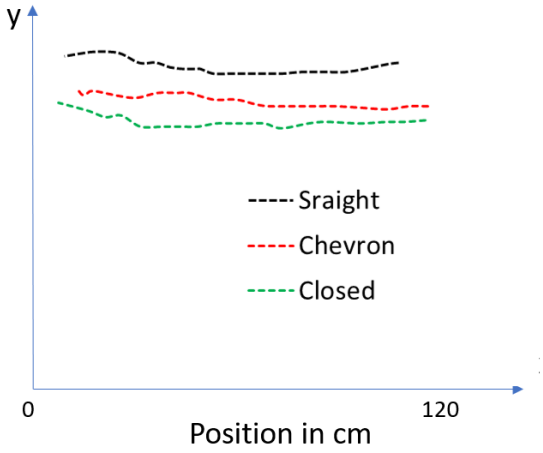

FIGURE 14. Straight trajectory traced by the closed, straight and chevron configurations.

B. EXPERIMENTAL RESULTS

The performance of the proposed controller is verified by carrying out experiments three different sets of experiments. The first set of experiments was conducted in teleportation mode to check the mobility of the platform and effect of steering angle on the platform velocity and to check the synchronization of the steering angle with the heading angle and performance of the heading controller. As all the three configurations of the platform are governed by the same differential based kinematic model, the same heading controller is used for each configuration. Figure 13 shows the position tracking of the CG of each configuration while moving from one point to another.

The performance of the IMU-based heading error controller tested for three different configurations. For evaluating the point to point locomotion performance of the platform, the robot was located at the start point of the path with the steering angle of both wheels as same as the desired heading angle. The constant heading angle is achieved by IMU feedback. The heading of the robot was measured by using a 9-axis inertial measuring unit consisting of an accelerometer, gyroscope, and a magnetometer in the following manner. The roll and pitch angles are estimated by combining a 3-axis accelerometer and a 3-axis gyros with a complementary filter. The complementary filter consists of both high-pass and low-pass filters. The low pass filter filters high-frequency signals in accelerometer and low pass filters that filter low-frequency signals such as the drift of the gyroscope. By combining these filters, the roll and pitch angle is obtained, which is further combined with magneto sensor data to obtain the heading of the platform. Figure 14 and 15 show the trajectory traced by the closed, straight, and chevron configurations. Experimental data shows a slight variation in the heading angle, which is due to modeling errors, environmental disturbances, and parameter uncertainties.

In autonomous settings, the performance of the closed-loop controller with IMU based feedback and LIDAR based localization was evaluated using three different geometrical paths (straight line, pivot motion, and circular movement) are considered. A straight path with two waypoints as (0 cm, 0 cm), (110 cm, 110 cm), are considered. The circular path describes a circle with a radius of 0.55 meters. The robot central module is located exactly on the path. Both paths are supplied as a sequence of 50 points. These sequences of the waypoints and geometrical path information are passed to the robot and the controller estimates the corresponding heading angle and steering angle information. Evaluation of the performance of heading error was done using path following by getting the

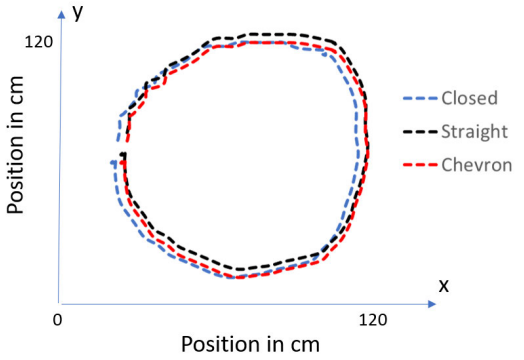

FIGURE 15. Circular trajectory traced by the closed, straight and chevron configurations.

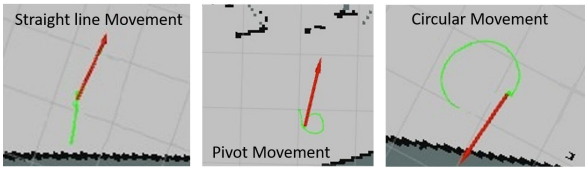

FIGURE 16. Trajectory obtained from the LIDAR data for the straight configuration.

LIDAR positions. Figure 16 shows the trajectory information including the straight-line, in-plane pivot and circular trajectory with a closed-loop controller for the straight configuration.

Remark: It should be noted that any change in the robot configuration also changes its ability to track a given trajectory. For example, the configurations are shown in Fig. 5(a), and 5(c) does not hamper in the ability of the robot to follow a circular path after the wheel alignment is corrected to zero. However, the wheel alignment alone may not be able to provide satisfactory circular path tracking, if the robot configuration is similar to Fig. 5(b). It was observed during simulations and experiments that, a small adjustment in wheel alignment (30 degree) was necessary to achieve a satisfactory path tracking. The solution to this issue is the subject of future work.

VII. CONCLUSION

The work presented a state of the art autonomous robot platform hTrihex for floor cleaning tasks. The critical aspects like mechanical design, electronic design, autonomy are demonstrated, and kinematics equations for different configurations are derived. A novel robust backstepping design is proposed for motion control, whose effectiveness is verified through numerical simulations and experiments. Future research on hTrihex will be focused on the following areas: implementation of the optimal design of the cleaning module, designing of the wheel for reducing the slip and drag on the various type of floors, developing an advanced controller to deal with the variation of the moment of inertia of the platform during locomotion and reconfiguration.

ACKNOWLEDGMENT

This research was supported by the National Robotics Programme under its Robotics Enabling Capabilities and Technologies (Funding Agency Project No. 192 25 00051), National Robotics Programme under its Robot Domain Specific (Funding Agency Project No. 192 22 00058) and administered by the Agency for Science, Technology and Research.

REFERENCES

[1] H. Choset, "Coverage for robotics–a survey of recent results," *Ann. Math. Artif. Intell.*, vol. 31, nos. 1–4, pp. 113–126, 2001.

[2] R. H. Peck, J. Timmis, and A. M. Tyrrell, "Omni-pi-tent: An omni-directional modular robot with genderless docking," in *Proc. Annu. Conf. Towards Auton. Robot. Syst.* Cham, Switzerland: Springer, 2019, pp. 307–318.

[3] H. Wei, Y. Cai, H. Li, D. Li, and T. Wang, "Sambot: A self-assembly modular robot for swarm robot," in *Proc. IEEE Int. Conf. Robot. Autom.*, May 2010, pp. 66–71.

[4] G. Studer and H. Lipson, "Spontaneous emergence of self-replicating structures in molecube automata," in *Proc. 10th Int. Conf. Simulation Synth. Living Syst. (Artif. Life X)*. London, U.K.: MIT Press, 2006, pp. 227–233.

[5] A. Kamimura, E. Yoshida, S. Murata, H. Kurokawa, K. Tomita, and S. Kokaji, "A self-reconfigurable modular robot (MTRAN)—Hardware and motion planning software—," in *Distributed Autonomous Robotic Systems 5*. Cham, Switzerland: Springer, 2002, pp. 17–26.

[6] M. Yim, D. G. Duff, and K. D. Roufas, "PolyBot: A modular reconfigurable robot," in *Proc. ICRA. Millennium Conf. IEEE Int. Conf. Robot. Automat. Symp.*, vol. 1, Apr. 2000, pp. 514–520.

[7] V. Prabakaran, M. R. Elara, T. Pathmakumar, and S. Nansai, "Floor cleaning robot with reconfigurable mechanism," *Autom. Construct.*, vol. 91, pp. 155–165, Jul. 2018.

[8] R. Parween, V. Prabakaran, M. R. Elara, A. Vengadesh, and V. Sivanantham, "Application of tiling theory for path planning strategy in a polyiamond inspired reconfigurable robot," *IEEE Access*, vol. 7, pp. 6947–6957, 2019.

[9] R. Parween, Y. Shi, K. Parasuraman, A. Vengadesh, V. Sivanantham, S. Ghanta, and R. E. Mohan, "Modeling and analysis of hHoneycomb—A polyhex inspired reconfigurable tiling robot," *Energies*, vol. 12, no. 13, p. 2517, 2019.

[10] P. Veerajagadheswar, V. Sivanantham, M. Devarassu, and M. R. Elara, "Htetran—A polyabolo inspired self reconfigurable tiling robot," in *Proc. IEEE/RSJ Int. Conf. Intell. Robots Syst. (IROS)*, Nov. 2019, pp. 4877–4884.

[11] T. T. Tun, L. Huang, R. E. Mohan, and S. G. H. Matthew, "Four-wheel steering and driving mechanism for a reconfigurable floor cleaning robot," *Autom. Construct.*, vol. 106, Oct. 2019, Art. no. 102796.

[12] Y. Shi, M. Rajesh Elara, A. Vu Le, V. Prabakaran, and K. L. Wood, "Path tracking control of self-reconfigurable robot hTetro with four differential drive units," 2019, *arXiv:1911.08746*. [Online]. Available: http://arxiv.org/abs/1911.08746

[13] A. Le, M. Arunmozhi, P. Veerajagadheswar, P.-C. Ku, T. H. Minh, V. Sivanantham, and R. Mohan, "Complete path planning for a tetris-inspired self-reconfigurable robot by the genetic algorithm of the traveling salesman problem," *Electronics*, vol. 7, no. 12, p. 344, Nov. 2018.

[14] A. Manimuthu, A. V. Le, R. E. Mohan, P. Veerajagadeshwar, N. H. K. Nhan, and K. P. Cheng, "Energy consumption estimation model for complete coverage of a tetromino inspired reconfigurable surface tiling robot," *Energies*, vol. 12, no. 12, p. 2257, Jun. 2019.

[15] A. Le, P.-C. Ku, T. Than Tun, N. H. K. Nhan, Y. Shi, and R. Mohan, "Realization energy optimization of complete path planning in differential drive based self-reconfigurable floor cleaning robot," *Energies*, vol. 12, no. 6, p. 1136, Mar. 2019.

[16] A. V. Le, N. H. K. Nhan, and R. E. Mohan, "Evolutionary algorithm-based complete coverage path planning for tetriamond tiling robots," *Sensors*, vol. 20, no. 2, p. 445, Jan. 2020.

[17] A. Le, V. Prabakaran, V. Sivanantham, and R. Mohan, "Modified A-Star algorithm for efficient coverage path planning in tetris inspired self-reconfigurable robot with integrated laser sensor," *Sensors*, vol. 18, no. 8, p. 2585, Aug. 2018.

[18] H. Fukuda, C. Kanomata, N. Mutoh, G. Nakamura, and D. Schattschneider, "Polyominoes and polyiamonds as fundamental domains of isohedral tilings with rotational symmetry," *Symmetry*, vol. 3, no. 4, pp. 828–851, Dec. 2011.
[19] S. W. Golomb, *Polyominoes: Puzzles, Patterns, Problems, and Packings*. Princeton, NJ, USA: Princeton Univ. Press, 1996.
[20] C. Larson, "Combinatorial properties of polyiamonds," CUNY Acad. Works, City Univ New York, New York, NY, USA, Tech. Rep., 2014. [Online]. Available: https://academicworks.cuny.edu/gc_etds/441
[21] M. M. Rayguru, S. Roy, and I. N. Kar, "Time-scale redesign-based saturated controller synthesis for a class of MIMO nonlinear systems," *IEEE Trans. Syst., Man, Cybern. Syst.*, early access, Oct. 18, 2019, doi: 10.1109/TSMC.2019.2945841.
[22] M. M. Rayguru and I. N. Kar, "Contraction theory approach to disturbance observer based filtered backstepping design," *J. Dyn. Syst., Meas., Control*, vol. 141, no. 8, Aug. 2019, Art. no. 084501.

RIZUWANA PARWEEN (Member, IEEE) received the bachelor's and master's degrees in mechanical engineering from the National Institute of Technology Rourkela, India, and the Ph.D. degree from the Indian Institute of Science, Bengaluru, India. She has over two years of industrial experience, as a Product Development Engineer with KSB Tech Private Ltd., Pune, and a Structural Analyst with Cummins, Pune. As a Postdoctoral Research Fellow with SUTD, she worked on the design and development of Unloader Knee Brace for Asian Patients, in collaboration with physicians with the Changi General Hospital, Singapore. She is currently a Research Fellow with the Engineering Product Development Pillar, Singapore University of Technology and Design (SUTD). She is also a Research Fellow in design, development, and modeling of the self-reconfigurable floor cleaning robots.

MANUEL VEGA HEREDIA received the degree in electromechanical engineering, the master's degree in industrial engineering, and the Ph.D. degree in engineering sciences, (Robotics) from the Autonomous University of Ciudad Juárez, Mexico, in 2016. He was a Postdoctoral Research Fellow with the Singapore University of Technology and Design, from 2018 to 2020. He is currently a Full-Time Professor with the Universidad Autonoma de Occidente.

MADAN MOHAN RAYGURU received the B.Tech. degree from BPUT, India, the master's degree in electrical engineering from NIT Roukela, and the Ph.D. degree in control systems from the Indian Institute of Technology, Delhi, India. He is currently a Research Fellow with the Engineering Product Development Pillar, Singapore University of Technology and Design (SUTD). His research interests include robotics, convergent systems, and saturated controller design.

RAIHAN ENJIKALAYIL ABDULKADER received the bachelor's degree in electronics and communication from the University of Calicut, India, in 2016, and the master's degree in robotics from SRM University, India, in 2019. He is currently a Visiting Fellow with the Singapore University of Technology and Design under the guidance of Dr. M. R. Elara. His research interests include system autonomy for floor cleaning and vertical climbing application.

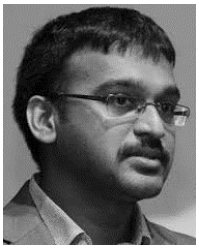

MOHAN RAJESH ELARA received the B.E. degree from the Amrita Institute of Technology and Sciences, Bharathiar University, India, and the M.Sc. degree in consumer electronics and the Ph.D. degree in electrical and electronics engineering from the Nanyang Technological University, Singapore. He was a Lecturer with the School of Electrical and Electronics Engineering, Singapore Polytechnic. He is currently an Assistant Professor with the Engineering Product Development Pillar, Singapore University of Technology and Design (SUTD). He is also a Visiting Faculty Member with the International Design Institute, Zhejiang University, China. He has published more than 80 papers in leading journals, books, and conferences. He has served in various positions of organizing and technical committees of over twenty international competitions and conferences. His research interests include robotics with an emphasis on self-reconfigurable platforms and research problems related to robot ergonomics and autonomous systems. He was a recipient of the SG Mark Design Award, in 2016, 2017, and 2018, the A'Design Award, in 2018, the ASEE Best of Design in Engineering Award, in 2012, and the Tan Kah Kee Young Inventors' Award, in 2010.